https://dx.doi.org/10.1016/j.conbuildmat.2023.134562
This is the Pre-Published Version.

Cooling efficiency of thermochromic asphalt pavement material and its contribution to field performance enhancement of asphalt mixture

Zihao Chen[a, b], Henglong Zhang[a, c]*, Xue Yang [a], Zhen Leng [b]**, Yunhong Tang [a]

[a] Key Laboratory for Green & Advanced Civil Engineering Materials and Application Technology of Hunan Province, College of Civil Engineering, Hunan University, Changsha 410082, China; [b] Department of Civil and Environmental Engineering, The Hong Kong Polytechnic University, Hong Kong 999077, China; [c] Hunan Provincial Engineering Research Center for Construction Solid Wastes Recycling, Hunan Yunzhong Recycling Technology Co., Ltd, Changsha 410205, China

Abstract

The thermochromic asphalt pavement material (TAPM) has the potential to bilaterally regulate the pavement temperature according to seasonal environment, which is beneficial to heat island effect mitigation and pavement performance enhancement. However, studies on quantifying the cooling efficiency and verifying the field performance of TAPM are still limited. This study aims to more extensively verify the cooling efficiency of TAPM in different climatic regions and to reveal its cooling mechanism in the field. The key thermophysical parameter, solar albedo, of TAPM was back-calculated using an interpolation methodology to match the numerical simulation results with the specimen temperature data monitored experimentally. The cooling efficiency of TAPM in broader climatic regions was demonstrated through the numerical simulation combined with real meteorological conditions. In view of the

© 2023. This manuscript version is made available under the CC-BY-NC-ND 4.0 license http://creativecommons.org/licenses/by-nc-nd/4.0/

cooling characteristics of TAPM as well as the temperature dependency attribute of asphalt mixture, various field performance properties of TAPM were characterized. It was found that at a temperature larger than 31 ℃, the solar albedo of TAPM is 0.30, which is six times larger than that of the conventional asphalt pavement material, indicating a strong reflection ability to solar radiation. The average temperature reduction of TAPM compared with the conventional asphalt pavement material in different regions is 6.26 ℃ with a standard deviation of 0.79 ℃, demonstrating the effective, universal and stable cooling effect of TAPM in summer across China. The cooling function of TAPM contributes to the improvement of high-temperature stability, aging resistance and low-temperature cracking performance of asphalt mixture. Therefore, it is necessary to consider the unique cooling function of TAPM for a more objective evaluation of its field performance.

Keywords: cool pavement material; thermochromic microcapsule; solar albedo back calculation; numerical simulation; cooling efficiency; field performance enhancement.

1. Introduction

Asphalt binder, which features an extremely low solar albedo due to its intrinsic black or dark brown color, allows the asphalt pavement to easily absorb a considerable amount of thermal energy from solar radiation in summer and then leads to undesirably high service temperature of pavement [1, 2]. On one hand, the high-temperature and aging-related pavement distresses tend to become more serious, which compromises the service quality and longevity of asphalt pavement [3-5]. On the other hand, the high surface temperature of asphalt pavement also intensifies the urban heat island effect,

and further worsens the urban microclimate by exacerbating the energy consumption and pollutant gas emissions [6-10]. Therefore, developing cool pavement technologies to reduce the excessively high service temperature of asphalt pavement in summer can not only enhance the field performance of asphalt pavement but also mitigate the urban heat island effect.

According to the heat transfer principle, the temperature distribution in asphalt pavement is a coupled result of the heat conduction along asphalt pavement structure depth and the heat exchange between asphalt pavement surface and external natural environment in the form of radiation and convection [11]. Meteorological conditions to which the asphalt pavement is exposed and the thermophysical parameters possessed by pavement materials are two paramount aspects that determine the temperature field of asphalt pavement [12]. Compared with arbitrarily variable meteorological conditions like air temperature, solar radiation intensity, wind speed and sunshine hours, the thermophysical parameters including solar albedo, thermal conductivity, specific heat capacity and emissivity are more readily artificially-controlled through adjusting the volumetric design of asphalt mixture or applying specific cooling materials [6-8].

Based on different cooling mechanisms, various forms of cool pavement, including evaporative pavement, thermal resistance pavement, phase change pavement and reflective pavement, have been developed [6-8]. Differing from the first three cool pavement types all of which just passively dissipate, block or transfer heat after the thermal flux has entered into the pavement structure, the reflective pavement can directly curtail the amount of heat entrance through raising the solar albedo of pavement.

Some literature has also reported that among various thermophysical parameters, it is the solar albedo that imposes the most significant effect on the temperature field of pavement [13]. Therefore, the reflective pavement is regarded as one of the most efficient and promising cool pavement types [14, 15].

However, as a result of the fixed high solar albedo, the conventional reflective coating imposes the same cooling effect on the pavement in winter just as in summer. The low-temperature field performance of pavement will be further compromised given that the cooling function of conventional reflective coating makes negative impacts in winter [16-18]. In view of the limitation of the static solar reflectance of conventional reflective coating, a smarter reflective pavement material that can present dynamically changeable solar reflectance in response to ambient temperature has been developed through the application of thermochromic microcapsules into asphalt binder.

The colored thermochromic microcapsules can change into the colorless state as the ambient temperature rises over the certain threshold value, while turning back into the original color when the ambient temperature declines below this critical temperature. The thermochromism response of thermochromic microcapsule is attributed to the encapsulated three-component compound that is composed of chromophore, color developer and solvent [19-21]. The solvent is a temperature sensitive material of which phase change is responsible for the electron transfer between chromophore and color developer. The electronic gain or loss for chromophore can lead to its own molecular structure change. Meanwhile, the reflectance of chromophore in visible spectrum is correspondingly changed with the variation of chromophore molecular structure, which

macroscopically results in the thermochromic phenomenon of compound.

The visible light accounts for more than 40% of solar radiation energy [22]. It is also in the visible spectrum that the reflectance of thermochromic microcapsules thermally responds, so that the thermochromic microcapsules are able to efficiently adjust the amount of solar radiation absorption in accordance with ambient temperature [23]. When modified by thermochromic microcapsules, the asphalt pavement material can present the similar dynamically changeable optical response by which the thermochromic asphalt pavement material (TAPM) can increase the solar albedo to strengthen its cooling effect on asphalt pavement in summer but reduce the solar albedo to weaken the cooling effect in winter [17, 18].

So far, the research work on thermochromic asphalt materials is still at the early stage, mainly focusing on the basic field performance evaluation of this kind of cool pavement material and the verification of its cooling effect on pavement [21, 24-28]. In terms of these two aspects, there still exist some issues that deserve more attention.

First of all, the existing studies usually directly verified the cooling effect of TAPM by means of comparing the temperature differences between asphalt mixture samples with and without thermochromic microcapsules in outdoor solar radiation test or indoor radiation simulation test [24-28]. However, the cooling efficiency outcomes evaluated by this way are highly dependent on the specific environment conditions in radiation test. The temperature-reduction effects of the thermochromic asphalt mixture sample relative to conventional asphalt mixture sample show significant discrepancies in different studies, because the outdoor meteorological conditions or indoor simulation

conditions are not fully consistent in different studies. As a result, the cooling efficiency outcomes of TAPM obtained from different studies cannot be unified with or verified by each other. The outcomes, produced from regional outdoor natural environment or limited indoor simulation environment, cannot be universally representative for the cooling efficiency of TAPM in different climatic regions. A more extensive verification of cooling efficiency is necessary for this kind of pavement material.

In comparison, the parameter of solar albedo of asphalt mixture, although its value is gradually increased due to the field aging effect [29, 30], is still an intrinsic thermophysical property that is independent on testing environment and becomes an important material parameter input in the numerical simulation for pavement temperature field. If the solar albedo of thermochromic asphalt mixture was obtained, the cooling efficiencies of this kind of cool pavement material in different climatic regions could be more readily verified through the numerical simulation combined with real meteorological conditions from database. Unfortunately, asphalt mixture, as a multiphase material, is not easily fabricated to be the geometric size and shape that are suitable for spectrophotometer test, which makes it really difficult to precisely measure the reflectance spectrum of asphalt mixture. The solar albedo of TAPM, hence, cannot be accurately calculated by the integral formula involved with asphalt mixture reflectance spectrum and solar radiation distribution. In addition, the solar albedo could also be measured using a field method such as an albedometer. However, this field method is more suitable for testing the solar albedo at the scale of pavement rather than the scale of asphalt mixture. Paving a certain length of experimental road is really a

challenge in most cases. As a consequence, in terms of the verification of cooling efficiency of TAPM, all existing studies tended to use the relative temperature reduction magnitude in radiation test to replace the comparison of solar albedo between modified and unmodified asphalt mixture samples [24-28].

Another issue is that the unique cooling effect of TAPM is seldom taken into account when the field performance of TAPM is evaluated. Unlike the commonly used polymer modifiers that improve the field performance of asphalt materials mainly through the formed polymer-asphalt two phase structure [31-34], the dual effects of thermochromic microcapsule on the field performance of asphalt pavement materials should be integrated. One is directly derived from the physical interaction between thermochromic microcapsule and asphalt matrix. In this case, the action mechanism of thermochromic microcapsule is similar to those of polymer modifiers. Another is mediately derived from the cooling pavement effect of thermochromic microcapsule. This is because viscoelastic behavior and aging susceptibility, both of which are representative temperature-dependent characteristics shown by asphalt road materials, make the service temperature of asphalt pavement become one of the most prominent factors on pavement material performance, structure response and service life [12, 35, 36]. The ignorance of the cooling pavement effect of thermochromic microcapsule may lead to an underestimation of the overall field performance of its modified asphalt pavement materials.

The objective of this research is to fill the research gaps about TAPM in its cooling efficiency verification and field performance evaluation aspects. An interpolation

method with the aim to minimize the error between the temperature field data collected from outdoor solar radiation test and calculated from numerical simulation was utilized to back-calculate the parameter of solar albedo for TAPM. The cooling efficiency of this kind of cool pavement material in broader climatic regions was further demonstrated through the numerical simulation combined with real meteorological conditions. Based on the temperature dependency attribute of asphalt materials in both viscoelastic property and aging susceptibility, the action modes of cooling effect of TAPM on the field performance of asphalt mixture were determined. Furthermore, the field performance comparisons of TAPM with and without consideration of its cooling efficiency were conducted to reveal the effects of cooling function on different field performance properties of this kind of cool pavement material.

2. Experiments, theories and simulation

2.1 Materials

The thermochromic microcapsule used in this research is composed of fluorane dye (chromophore), bisphenol A (color developer), methyl stearate (solvent) and melamine-formaldehyde resin (shell material), and has the thermochromic temperature of 31 ºC and the specific gravity around 0.25. Additionally, the particle size distribution of thermochromic microcapsule is between 2 and 10 μm. The appearance color of thermochromic microcapsule and the molecular structure of chromophore below and above 31 ºC have been illustrated in the literature [23]. It can be known that when the ambient temperature rises over the transition temperature, the molecular structure of chromophore transforms from quinonoid structure to lactone structure while the color

of thermochromic microcapsule also changes from red to colorless state. The opposite changes in molecular structure and appearance color occur when the ambient temperature declines below the transition temperature again.

The base asphalt with a penetration grade of 60/80 was used, and its basic properties are presented in Table 1. The specific preparation process of thermochromic asphalt binder is that the 6% dosage of thermochromic microcapsules were mixed with base asphalt at 150 ºC for 60 min at the shearing speed of 4,000 rpm. As control asphalt binder, the pure asphalt without thermochromic microcapsule went through the same shearing process as thermochromic asphalt binder.

Two types of asphalt mixtures were prepared with thermochromic asphalt binder and control asphalt binder, which are named as modified sample and control sample, respectively. The asphalt mixture type of AC-13 was selected, and the coarse, fine aggregates and mineral filler were limestone. The optimal binder content for modified sample was determined as 5.15% according to the Marshall asphalt mixture design method. For simplicity, the same binder content was adopted for control sample.

Table 1. Basic properties of base asphalt

Properties	Measured values
Penetration (25 ºC, dmm)	65
Softening point (ºC)	46.3
Ductility (15 ºC, cm)	> 150
Viscosity (135 ºC, mPa·s)	434.1

2.2 Reflectance spectrum test

The ultraviolet-visible-near infrared spectrophotometer with a spectral scanning limit from 200 to 1200 nm was employed to qualitatively evaluate the thermal responses of thermochromic microcapsule and its modified asphalt mixture in reflectance spectrum. Since the geometric size and shape requirements by optical device, the compacted asphalt mixture specimens are not suitably used as testing samples in spectral scanning tests. In view of this limit, a certain number of coarse aggregates with appropriate size and shape were selected from loose asphalt mixtures to substitute for the compacted asphalt mixture specimens for qualitative analysis of optical property. In order to obtain the reflectance spectrum below and above the thermochromic temperature, the samples should be thermostatically conditioned before spectral test for 20 min at 25 ºC and 35 ºC, respectively.

2.3 Outdoor solar radiation test

In outdoor solar radiation test, the modified sample and control sample were fabricated to be the standard Marshall specimens. The thermocouples were inserted inside the specimens at the location of 2 cm beneath the specimen top surface. Except the top surface, the other surfaces of specimen were coated by polyurethane thermal insulator to enable the heat flux in specimen only to transmit vertically. The diagram of outdoor solar radiation test is illustrated as Fig. 1. The specimens were placed outside for successive three days in hot summer, and the temperature data inside specimens were collected.

Fig. 1. Specimens for outdoor solar radiation test.

2.4 Numerical simulation for outdoor solar radiation test

2.4.1 Heat transfer theory of asphalt pavement

The modes of heat transfer are usually classified into radiation, convection and conduction [11]. The heat transfer between natural environment and pavement structure take place on the pavement surface in the form of radiation and convection, including solar direct and diffuse radiation (the sum of two parts is called total solar radiation), atmospheric radiation, long-wave radiation emitted outwards by pavement, heat convection between pavement surface and air flow. The thermal equilibrium equation on the pavement top surface is presented as equation (1).

$$Q=(1-\mu)Q_s+Q_{sky}-Q_{sur}-Q_h \quad (1)$$

where Q represents the net heat flux into pavement structure, W/m^2; Q_s represents the total solar radiation intensity, W/m^2; Q_{sky} represents the atmospheric radiation intensity, W/m^2; Q_{sur} represents the long-wave radiation intensity, W/m^2; Q_h represents the heat convection intensity, W/m^2; and μ represents the solar albedo of pavement.

The difference between atmospheric radiation intensity and long-wave radiation intensity is equal to the effective pavement surface radiation intensity that can be

expressed as equation (2). According to Newton's law of cooling, the expression of heat convection intensity is shown by equation (3).

$$Q_{eff}=Q_{sky}-Q_{sur}=\varepsilon\sigma[(T_{air}-T_z)^4-(T_{sur}-T_z)^4] \quad (2)$$

$$Q_h=h(T_{sur}-T_{air}) \quad (3)$$

where Q_{eff} is the effective pavement surface radiation intensity, W/m^2; ε represents the radiation emissivity of pavement surface; σ is Stefan-Boltzmann constant that is equal to 5.67×10^{-8}, W/(m^2·K^4); T_{sur}, T_{air} and T_z represent the temperature of pavement surface, the air temperature, and the absolute zero temperature, ºC; and h is the convection coefficient that is related to wind speed, W/(m^2·ºC).

Additionally, the heat flux that enters into the pavement structure is further transmitted along the pavement depth in the form of conduction, which enables the temperature distribution inside the pavement to be a function of time and location. Based on both Fourier law (equation (4)) and the energy conservation law, the differential equation of heat conduction in pavement without internal heat source can be expressed as equation (5).

$$q=-\lambda grad T_{pav} \quad (4)$$

$$\frac{\partial T_{pav}}{\partial t}=\frac{\lambda}{\rho c}\left(\frac{\partial^2 T_{pav}}{\partial^2 x}+\frac{\partial^2 T_{pav}}{\partial^2 y}+\frac{\partial^2 T_{pav}}{\partial^2 z}\right) \quad (5)$$

where q is the heat flux vector; λ, ρ, c are the thermal conductivity, density and specific heat capacity of pavement material; T_{pav} is the pavement temperature; $grad T_{pav}$ represents the temperature gradient in pavement; t is the time; and x, y, z are the spatial coordinates.

It is worth noting that the testing specimens in outdoor solar radiation test follow

the same heat transfer theory as asphalt pavement.

2.4.2 Geometric model and boundary conditions in finite element simulation

The numerical simulation for outdoor solar radiation test was performed with the aid of finite element software (ABAQUS). The geometric model in simulation was established according to the real geometric size of specimens in outdoor solar radiation test. Then the geometric model was meshed using the element type of 4-node linear heat transfer tetrahedron. The meteorological data for those three days when the outdoor solar radiation test was carried out, including the hourly air temperature, average wind speed, daily sum of solar radiation, sunshine hours, etc., was collected from meteorology database system. Based on these meteorological data, the various heat transfer boundaries that are listed in the right side of equation (1) were written with the ABAQUS subroutine in accordance with the literature [37] and then loaded on specimens. The heat transfer boundaries on the specimen top surface were only taken into account because the other surfaces of specimen were wrapped by polyurethane thermal insulator. The geometric model and boundary conditions in numerical simulation are presented in Fig. 2. The temperature data at the node that is located at 2 cm beneath the specimen top surface was extracted from the simulation results.

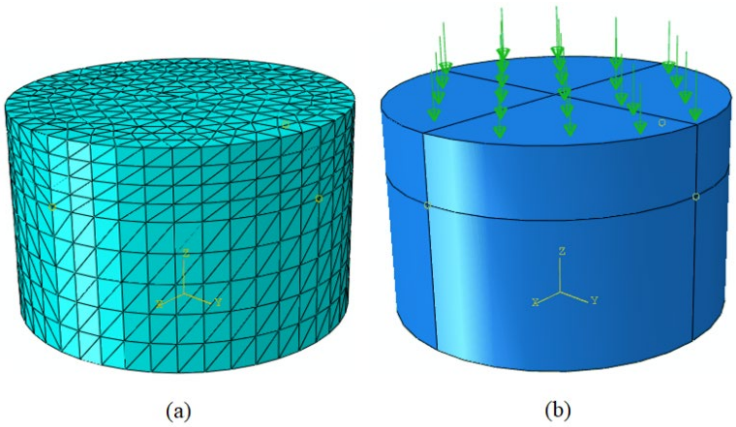

Fig. 2. The geometric model and boundary conditions in numerical simulation: (a) geometric size and mesh partition and (b) boundary conditions.

2.5 Experimental and theoretical methodologies for field performance

2.5.1 Dynamic modulus master curve

In this research, the constitutive model of 2S2P1D that consists of two springs, two parabolic elements and a dashpot (shown as Fig. 3) was used to characterize the viscoelastic behavior of asphalt mixture. Based on the 2S2P1D model, the expression of complex modulus, dynamic modulus, storage modulus and loss modulus can be presented as equations (6)-(11) [38].

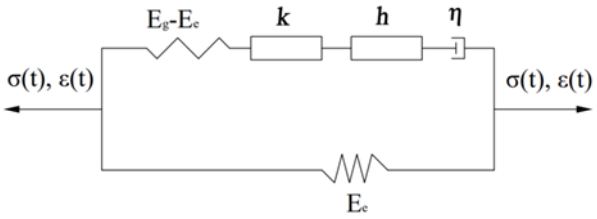

Fig. 3. The 2S2P1D model.

$$E^*(\omega)=E_e+\frac{E_g-E_e}{1+\alpha(i\omega\tau_0)^{-k}+(i\omega\tau_0)^{-h}+(i\omega\beta\tau_0)^{-1}} \quad (6)$$

$$E^*=E^{'}+iE^{''},\ |E^*|=\sqrt{E^{'2}+E^{''2}} \quad (7)$$

$$E^{'}=E_e+\frac{(E_g-E_e)(1+A)}{(1+A)^2+B^2} \quad (8)$$

$$E^{''}=\frac{(E_e-E_g)B}{(1+A)^2+B^2} \tag{9}$$

$$A=\alpha(\omega\tau_0)^{-k}\cos(k\pi/2)+(\omega\tau_0)^{-h}\cos(h\pi/2) \tag{10}$$

$$B=-\alpha(\omega\tau_0)^{-k}\sin(k\pi/2)-(\omega\tau_0)^{-h}\sin(h\pi/2)-(\omega\beta\tau_0)^{-1} \tag{11}$$

where E^*, $|E^*|$, $E^{'}$, $E^{''}$, E_g, E_e are the complex modulus, dynamic modulus, storage modulus, loss modulus, glass modulus and equilibrium modulus; ω is the angular frequency, and $\omega=2\pi f$, f is the frequency; α, k, h, β, τ_0 are model coefficients, and $\eta=(E_g-E_e)\beta\tau_0$.

The viscoelastic properties of asphalt mixture are dependent on both time and temperature conditions, and follow the time-temperature superposition principle (TTSP). The WLF equation (equation (12)) was used to describe the time-temperature superposition relationship. Based on TTSP, the unknown coefficients in equations (6)-(12) can be solved with nonlinear least square method to make the error function (equation (13)) reach the minimum value. In this way, the dynamic modulus master curve at a certain temperature can be constructed.

$$\log a_T=\frac{-C_1(T-T_{ref})}{C_2+(T-T_{ref})} \tag{12}$$

$$F_{error}=\frac{1}{N}\sum_{i=1}^{N}\left|\frac{G^*_{m,i}-G^*_{c,i}}{G^*_{m,i}}\right| \tag{13}$$

where a_T is the horizontal shift factor, and $a_T=\omega_r/\omega=f_r/f$; f_r and ω_r are the reduced frequency and reduced angular frequency; T and T_{ref} are the testing temperature and reference temperature; C_1 and C_2 are coefficients that are related to T_{ref}; F_{error} is the error function; N is the number of data; and $G^*_{m,i}$ and $G^*_{c,i}$ are the measured dynamic modulus and calculated dynamic modulus, respectively.

In order to measure the dynamic moduli, the uniaxial compressive dynamic

modulus test within linear viscoelastic range was conducted on modified and control samples. The testing temperature ranges from -10 to 50 ºC with an increment of 15 ºC. The dynamic moduli at six loading frequencies (0.1, 0.5, 1, 5, 10 and 25 Hz) were collected at each testing temperature.

2.5.2 Real-time dynamic moduli during outdoor solar radiation test

The calculation method for the real-time dynamic moduli is based on the solved 2S2P1D model and WLF equation at a certain reference temperature. The solved WLF equation was firstly transformed into the equation (14) in which the coefficients of T_{ref}, C_1, C_2 had been known and f was set as 1.59 Hz (taking into account of the real velocity of vehicle on the road). Then a series of measured temperature data inside specimens during outdoor solar radiation test was substituted into the equation (14), and the corresponding reduced frequencies were calculated. In this case, the real-time dynamic moduli of asphalt mixture in response to its variable service temperature were obtained when the reduced frequencies were further substituted into the solved 2S2P1D model.

$$log f_r = \frac{-C_1(T-T_{ref})}{C_2+(T-T_{ref})} + log f \quad (14)$$

2.5.3 Relaxation spectrum and relaxation modulus

In linear viscoelastic theory of asphalt materials, the relaxation spectrum is deemed to be an indicator that contains the most fundamental viscoelastic information, and can be classified into continuous and discrete two types. As shown in equations (15) and (16), the relaxation modulus can be expressed in the form of continuous or discrete relaxation spectrum [38]. When the number of discrete relaxation time (parameter n in equation (16)) is large enough, the approximation relationship between continuous

relaxation spectrum and discrete relaxation spectrum can be shown as equations (17) and (18) [38]. Additionally, based on the relationship between continuous relaxation spectrum and complex modulus (equation (19)) as well as the constitutive model of 2S2P1D, the analytical expression of continuous relaxation spectrum can be presented as equations (20)-(22) [38]. Therefore, the continuous relaxation spectrum, discrete relaxation spectrum and relaxation modulus master curve can be solved in sequence once the coefficients in 2S2P1D model are determined.

$$E(t)=E_e+\int_{-\infty}^{\infty}H(\rho)e^{-t/\rho}dln\rho \tag{15}$$

$$E(t)=E_e+\sum_{j=1}^{n}E_j e^{-t/\rho_j} \tag{16}$$

$$E_j=H(\rho_j)\times\Delta ln\rho_j \tag{17}$$

$$\Delta ln\rho_j=\frac{1}{M}\ln 10 \tag{18}$$

$$H(\rho)=\pm\pi^{-1}ImE^*(i\omega)|_{i\omega\to\rho^{-1}e^{\pm i\pi}}=\pm\pi^{-1}ImE^*(\rho^{-1}e^{\pm i\pi}) \tag{19}$$

$$H(\rho)=\frac{(E_g-E_e)Y}{\pi(X^2+Y^2)} \tag{20}$$

$$X=1+\alpha\tau_0^{-k}\rho^k cos(k\pi)+\tau_0^{-h}\rho^h cos(h\pi)-\beta^{-1}\tau_0^{-1}\rho \tag{21}$$

$$Y=\alpha\tau_0^{-k}\rho^k sin(k\pi)+\tau_0^{-h}\rho^h sin(h\pi) \tag{22}$$

where $E(t)$ is the relaxation modulus, and t is the loading time; $H(\rho)$ represents the continuous relaxation spectrum, and ρ is the continuous relaxation time variant; ρ_j is the relaxation time of jth Maxwell unit in generalized Maxwell model; E_j represents the relaxation strength corresponding to ρ_j; M is the number of the discrete time assumed in each decade on the logarithmic scale; Im represents the operation of retaining the imaginary part of a complex-value function, and the variant of $i\omega$ in complex modulus function is replaced by $\rho^{-1}e^{\pm i\pi}$; and E_g, E_e, α, k, h, β, τ_0 are the coefficients in 2S2P1D

model.

2.5.4 Thermal stress during cooling process

During the cooling process, the produced thermal stress inside asphalt mixture can be calculated on the basis of the relaxation modulus master curve. According to the pavement thermal stress calculation formula proposed by Hills and Brien and the Boltzmann linear superposition principle, the accumulated thermal stress of asphalt mixture at the cooling time of τ can be calculated by equations (23) and (24) [39].

$$\sigma(\tau)=\int_0^{\tau}\frac{d(\varphi\Delta T)}{d\tau'}E\left(T_{ref},t'\right)d\tau' \tag{23}$$

$$t'=\int_0^{\tau-\tau'}\frac{dt}{a_T} \tag{24}$$

where $\sigma(\tau)$ is the sum accumulated thermal stress at the moment of τ; $E(T_{ref}, t')$ represents the relaxation modulus at the reduced time of t' and the reference temperature of T_{ref}; φ is the linear contraction coefficient of asphalt mixture, and assumed to be temperature-independent and equal to 1.7×10^{-5}; a_T is the shift factor of the temperature T relative to the reference temperature T_{ref}; ΔT is the temperature reduction amplitude during $d\tau'$, and in this research, the asphalt mixtures were cooled down from 20 to -20 ºC with a cooling rate of 5 ºC/h; and t' is the equivalent reduced time at the reference temperature, corresponding to the cooling duration from τ' to τ.

2.5.5 Low-temperature indirect tensile strength (ITS) test

According to the Chinese specification (JTG E20-2011 T 0716) for the low-temperature ITS test, the modified and control samples were fabricated to be the standard Marshall specimens and then thermally conditioned at -10 ºC for 1.5 h. The failure tensile strain values of specimens were collected from the ITS test with the

loading rate of 1 mm/min.

3. Results and discussion

3.1 Verification of cooling efficiency

3.1.1 Qualitative analysis of spectrum results

The reflectance spectra of thermochromic microcapsule in response to different temperatures are shown as Fig. 4 (a). It can be found that for thermochromic microcapsule, its reflectance spectra below and above 31 ºC display a major difference within the spectrum range from 350 to 700 nm while presenting almost no difference in ultraviolet and near infrared spectrum. This demonstrates the thermal response of thermochromic microcapsule in reflectance mainly occurs within the visible light range. In particular, the reflectance within the range of 375-560 nm is substantially increased by more than 50 % when the ambient temperature rises from below to above 31 ºC.

The reflectance spectra of modified and control asphalt mixture samples within the visible light range are also illustrated as Fig. 4 (b). It is clear that when the temperature varies from below to above 31 ºC, the modified sample shows a relatively more obvious increase in reflectance in comparison with control sample. This indicates the thermochromic microcapsule is able to effectively endow its modified asphalt mixture with its similar temperature-dependent reflection ability. In addition, the reflectance spectrum curve of modified sample is significantly higher than that of control sample at the temperature larger than 31 ºC, which further demonstrates the modification of thermochromic microcapsule is capable of improving the reflection ability of asphalt pavement materials against radiation at high temperatures. It should

be noted that due to the geometric size and shape limits on testing specimen by optical device, the differences in both scale and morphology inevitably exist between the specimen used in spectral scanning test and the real asphalt pavement surface. Therefore, the measured reflectance results herein are not used for accurately calculating the real solar albedo, but just for qualitatively illustrating the effect of thermochromic microcapsule on optical property of its modified asphalt mixtures.

The solar irradiance distribution is also presented in Fig. 4 (c). It can be seen that the solar irradiance is mainly centered around the wavelength of 500 nm. Interestingly, the spectral range where the thermochromic microcapsule and its modified asphalt mixture have the thermal response in reflectance is just consistent with the peak range of solar irradiance spectrum. This corresponding relationship causes the fact that for TAPM, its dynamic variation in reflectance spectrum can also give rise to the distinguished changes in its solar albedo. As a result, the TAPM presents the binary solar albedo values that are dependent on temperature, and has the potential to bilaterally regulate the pavement temperature in accordance with seasonal environment.

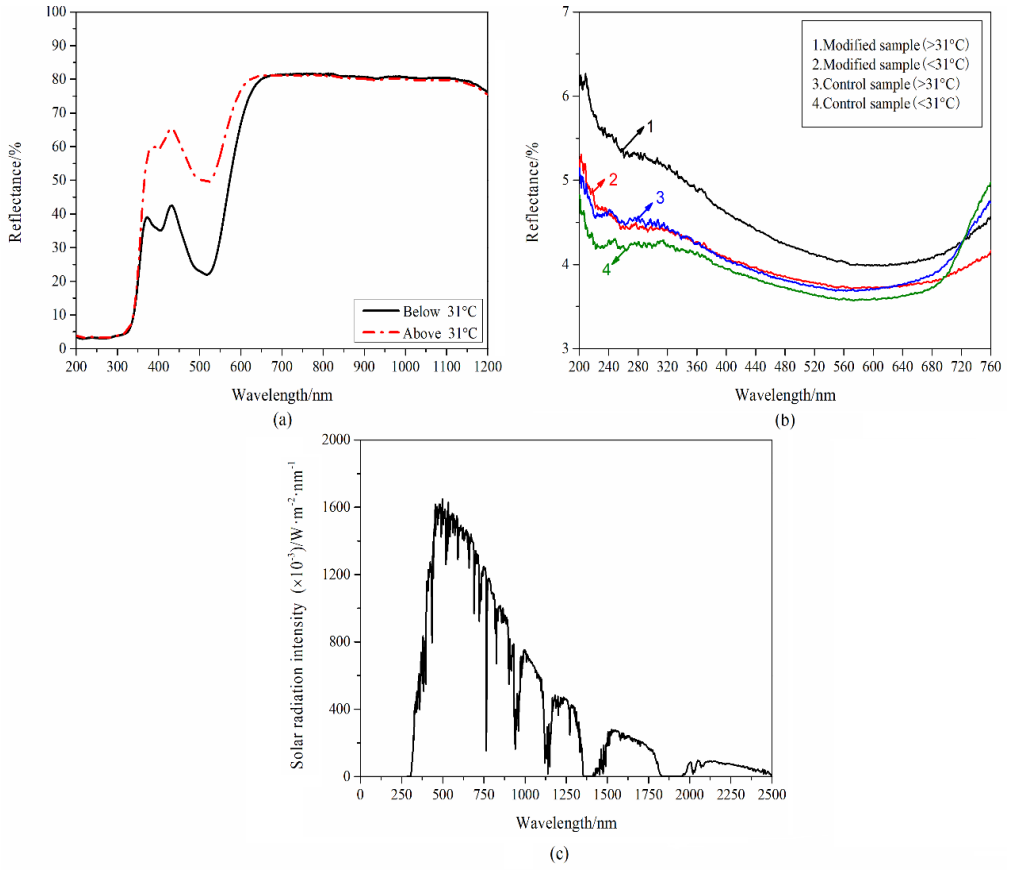

Fig. 4. The spectrum results: (a) the reflectance spectra of thermochromic microcapsule below and above 31 ºC, (b) the reflectance spectra of asphalt mixtures below and above 31 ºC and (c) solar irradiance spectrum.

3.1.2 Outdoor solar radiation test results

The outdoor solar radiation test results for successive three days in hot summer are shown by Fig. 5. Irrespective of sample types, the monitoring curve of specimen inner temperature over a day is similar to the changing trend of the air temperature with time, showing a bell-like shape with a temperature peak value at around 2:00 p.m. The maximum temperature of control sample nearly approximates to 65 ºC for each day while the maximum temperature of modified sample is not more than 60 ºC. It can be seen more clearly from Fig. 5 (b) that the modified sample has lower temperatures than control sample during the whole daytime, especially within the high-temperature period

from 11:00 a.m. to 4:00 p.m. And the maximum temperature of modified sample in the daytime can be lowered by 4-7 ℃ relative to the maximum temperature of control sample. The outdoor solar radiation test results verify the reflectance improvement of asphalt mixture brought by thermochromic microcapsule can indeed render the cooling effect to asphalt pavement in hot summer.

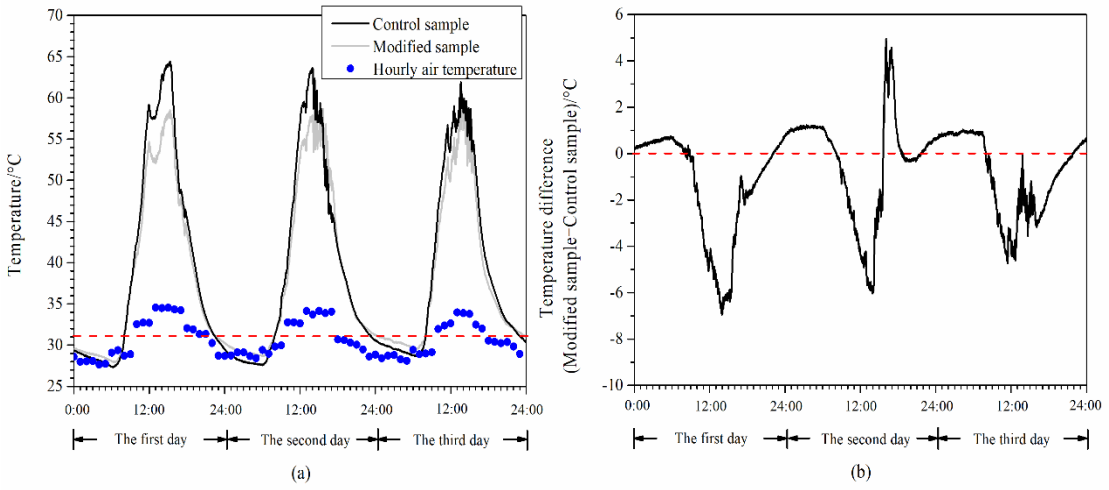

Fig. 5. The outdoor solar radiation test results: (a) the specimen inner temperatures monitored for successive three days and (b) the inner temperature differences between modified sample and control sample.

3.1.3 Back-calculation of solar albedo

According to the results in Section 3.1.1 and other literature [21, 40], it can be known that the thermochromic microcapsule mainly influences the solar albedo of asphalt mixture through its optically modifying effect, while showing no significant impacts on other thermophysical parameters. Furthermore, the influence of solar albedo on temperature field of pavement is also much greater than those of other thermophysical parameters [13]. Based on above two facts, one assumption can be made that both modified and control samples have the same thermophysical parameters

except solar albedo. The specific back-calculation procedures of solar albedo for thermochromic asphalt pavement are described as follows.

The thermophysical parameters of control sample were preset with reference to the values of conventional AC-13 pure asphalt mixture in other literature [37], and then the accuracy of parameters was verified by comparing errors between the simulated and measured data about the temperature of control sample during outdoor solar radiation test. Except solar albedo, the other thermophysical parameters of modified sample were set to be the same as those of control sample. Then, a probable range of solar albedo was estimated for modified sample, and a series of tentative solar albedo values were linearly interpolated within this range to find the value that can minimize the errors between specimen temperature data in outdoor solar radiation test and those from numerical simulation. This value was finally determined as the solar albedo of modified sample. Notably, all measured temperature data used in above calculation procedures was collected from outdoor solar radiation test in the third day. The data collected from the first two days was employed to further verify the calculation accuracy of thermophysical parameters of modified and control samples. In addition, the corresponding simulated data was obtained according to the method introduced in Section 2.4.

The thermophysical parameters of control sample (listed in Table 2) were set, and the accuracy of those parameters was evaluated according to Fig. 6. It can be found that the measured temperature curve and the simulated temperature curve have similar variation trends and are close to each other. The mean relative error (MRE) between the

measured data and the simulated data from 0 to 24 hours was calculated according to equation (25), and was used to evaluate the general fit degree between the measured data and the simulated data. The MRE is only 4.90 % that is less than 5%, which means the fit between the measured and simulated results is good, and the thermophysical parameters set for control sample are acceptable.

Table 2. Thermophysical parameters of asphalt mixtures

Thermophysical parameters	Control sample	Modified sample
Thermal conductivity (J/(m·h·°C))	4680	4680
Density (kg/m^3)	2400	2400
Specific heat capacity (J/(kg·°C))	925	925
Solar albedo	0.05	0.05, 0.10, 0.15, 0.20, 0.25, 0.30, 0.35, 0.40, 0.45, 0.50, 0.55
Emissivity	0.81	0.81

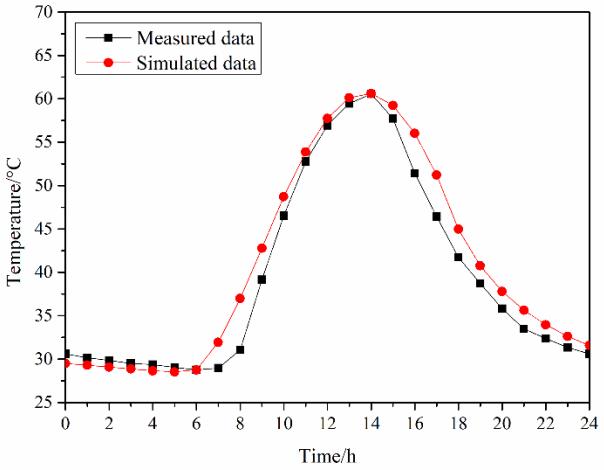

Fig. 6. The comparison of the simulated and measured data about the temperature of control sample in outdoor solar radiation test.

$$MRE=\frac{1}{25}\sum_{i=0}^{24}\left|\frac{T_{m,i}-T_{s,i}}{T_{m,i}}\right|\times 100\% \quad (25)$$

where i represents the time, h; $T_{m,i}$ represents the measured temperature data at time i, ℃; and $T_{s,i}$ represents the simulated temperature data at time i, ℃.

As shown in Table 2, the range of solar albedo estimated for modified sample was from 0.05 to 0.55, and the total eleven tentative values were linearly interpolated into this range with an interval of 0.05. The fitting results of the measured and the simulated data at different solar albedo tentative values can be seen in Fig. 7. As the solar albedo decreases from 0.55 to 0.05, the simulated daily maximum temperature of specimen is monotonously increased, and is closest to the measured value when the tentative solar albedo is equal to 0.30. Additionally, the change of MRE values between the measured data and the simulated data with the tentative solar albedo is presented as Fig. 7 (b). With the monotonous decline of solar albedo, the MRE decreases first and then increases, and reaches the minimum value of 4.27% when the solar albedo is interpolated to be 0.30.

It should be noted that differing form the control sample, the modified sample shows the dynamic reflection ability to solar radiation due to the optically modifying effect of thermochromic microcapsule. As a result, the modified sample should have two different solar albedo values when the sample temperature is larger or smaller than the thermochromic temperature of microcapsule, respectively. As shown in Fig. 5 (a), the surface temperature of modified sample is always larger than 31 ℃ when the modified sample is directly exposed to solar radiation during the daytime in hot summer. Therefore, the calculated solar albedo of 0.30 herein corresponds to the situation where

the sample temperature is larger than the thermochromic temperature of microcapsule.

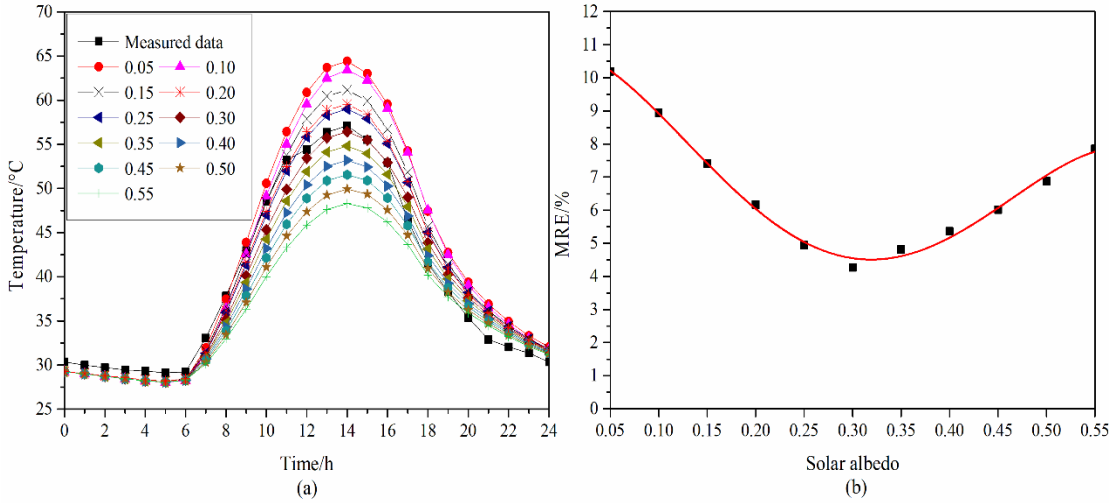

Fig. 7. The fitting results of the measured and the simulated data at different solar albedo tentative values: (a) the hourly temperature curve and (b) the MRE values.

In this research, the outdoor solar radiation test was carried out for successive three days. The data collected from the last day was used to back calculate the solar albedo of modified sample while the data collected from the first two days was used to verify the accuracy of those calculated thermophysical parameters for both modified and control samples. The fitting results of the measured and the simulated data in the first two days based on the calculated thermophysical parameters are presented in Fig. 8. It can be found that irrespective of modified or control sample, the simulated maximum temperatures are greatly close to the measured values, and the MRE values for twenty -five data in one day are all less than 5%. The good fitting results between the measured and the simulated data demonstrate the reliability of thermophysical parameters calculated for both modified and control samples. The solar albedo of modified sample is six times larger than that of control sample at temperatures larger than 31 ℃, which

essentially explains why the TAPM shows an effective cooling effect on pavement in hot summertime.

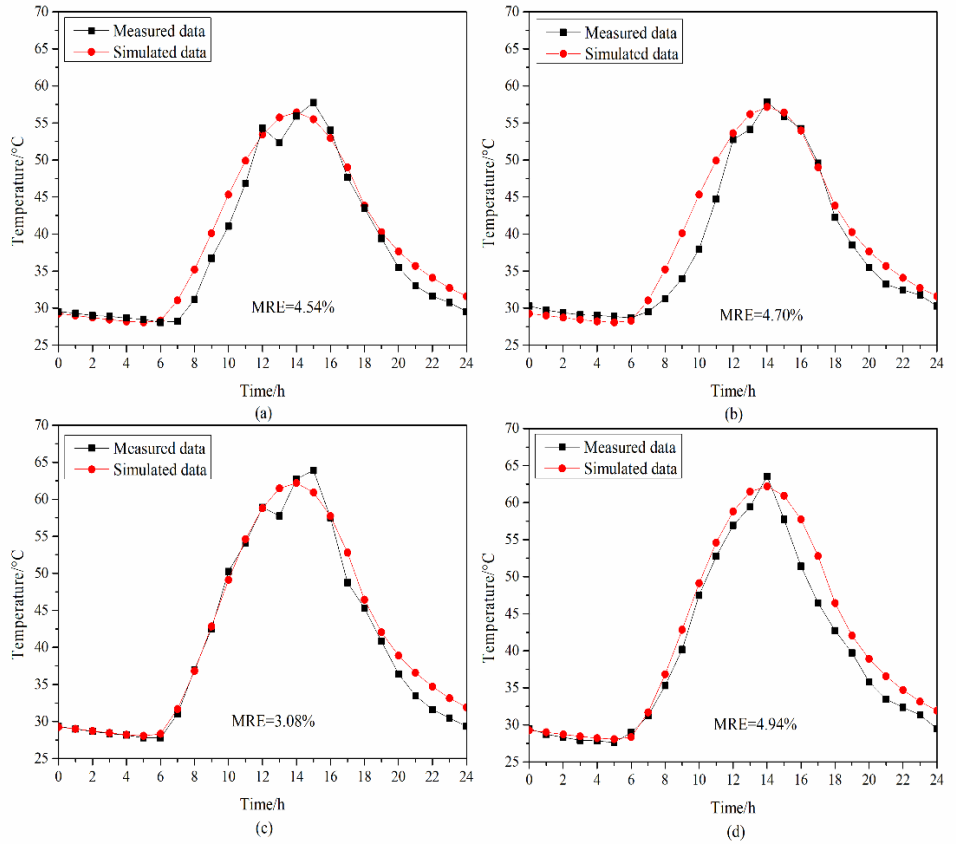

Fig. 8. The fitting results of the measured and the simulated data in the first two days: (a) the data of modified sample in the first day; (b) the data of modified sample in the second day; (c) the data of control sample in the first day and (d) the data of control sample in the second day.

3.1.4 Cooling efficiency evaluation in different climatic regions

After the determination of thermophysical parameters for modified and control samples, the temperature differences of pavement surface paved with modified and control sample in different climatic regions were further compared utilizing the numerical simulation combined with real meteorological conditions. The representative daily summer meteorology data of ten cities that are located in different climatic regions

of China were collected from database system and then transformed into the boundary conditions for numerical simulation of pavement temperature field. A typical pavement structure in China (shown as Fig. 9) was adopted in the simulation and the thermophysical parameters of pavement materials in different layers are listed in Table 3.

Since the pavement surface temperatures under the meteorological conditions in different climatic regions are not always larger than the thermochromic temperature of microcapsule, the solar albedo values of modified sample below and above 31 ℃ were simultaneously taken into account in the simulation through IF function in user subroutine. Since the TAPM is mainly used as a cool pavement material, the solar albedo of modified sample below 31 ℃ is less important than the value above 31 ℃. Additionally, the solar albedo below 31 ℃ cannot be back-calculated like the value above 31 ℃, due to the limitations of meteorological conditions in outdoor solar radiation test. For simplicity, the solar albedo of modified sample below 31 ℃ was set to be the same as control sample herein. Likewise, the temperature data at the location of 2 cm beneath the pavement surface was extracted from the simulation results.

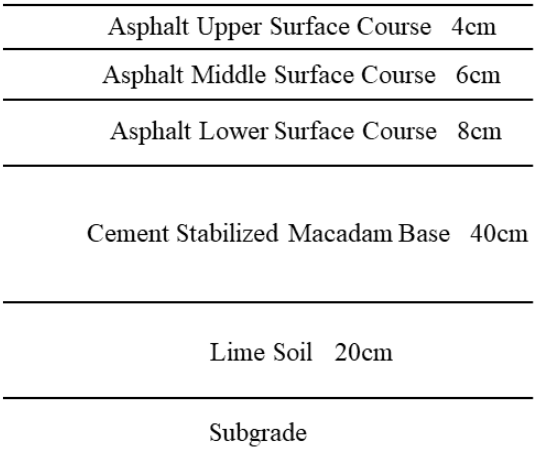

Fig. 9. Pavement structure model.

Table 3. Thermophysical parameters of pavement materials in different layers

Layers	λ	ρ	c	μ	ε
Upper Surface Course with Modified Sample	4680	2400	925	0.30/0.05	0.81
Upper Surface Course with Control Sample	4680	2400	925	0.05	0.81
Middle/Lower Surface Course	4680	2400	925	0.05	0.81
Cement Stabilized Macadam Base	5616	2200	912	0.05	0.81
Lime Soil	5148	2100	943	0.05	0.81
Subgrade	5616	1800	1040	0.05	0.81

Note: λ represents the thermal conductivity, J/(m·h·°C); ρ represents the density, kg/m^3; c represents the heat capacity, J/(kg·°C); μ represents the solar albedo; and ε represents the radiation emissivity.

Both meteorological conditions and the cooling efficiency of TAPM in different regions are summarized in Table 4. The variation ranges of maximum air temperature, total solar radiation intensity and average wind speed in ten regions are 21.01-37.82 ℃,

19.73-29.68 MJ and 1.00-2.77 m/s, indicating the summer meteorological conditions are selected widely and representatively. It can be also found that the maximum surface temperature of thermochromic asphalt pavement can be reduced by 4.90-7.62 ℃ relative to the maximum surface temperature of conventional asphalt pavement in different ten regions. The average cooling magnitude in ten regions reaches 6.26 ℃ with a standard deviation of 0.79 ℃, which indicates the TAPM is able to take the effective, universal and stable cooling effect on pavement in summer across China.

Table 4. Meteorological conditions and cooling efficiency of thermochromic asphalt pavement material in different regions.

Cities	$T_{air, max}$	$T_{air, min}$	V_{wind}	Q_{sol}	T_c	T_m	T_c-T_m
Harbin	29.87	22.84	1.88	19.73	46.38	41.48	4.90
Beijing	32.38	21.68	1.71	23.84	51.51	45.51	6.00
Zhengzhou	33.64	26	1.00	21.85	53.94	47.96	5.98
Changsha	37.82	28.38	1.27	25.58	60.40	53.73	6.68
Nanning	37.43	26.44	1.43	25.25	58.51	52.02	6.48
Nanjing	35.94	26.6	2.20	22.08	53.00	47.78	5.23
Chongqing	36.95	29.32	2.77	25.13	59.70	53.13	6.57
Kunming	25.94	17.36	1.82	23.65	45.73	39.80	5.93
Lhasa	21.01	10.75	1.05	27.60	46.49	38.87	7.62
Urumqi	24.03	14.95	2.02	29.68	48.06	40.82	7.24

Note: $T_{air, max}$ and $T_{air, min}$ represent the daily maximum and minimum air temperature, respectively, °C; V_{wind} represents the daily average wind speed, m/s; Q_{sol} represents the

daily total solar radiation intensity, MJ/m^2; T_c and T_m represent the daily maximum surface temperature of conventional asphalt pavement and modified asphalt pavement, respectively, °C; and T_c-T_m represents the temperature reduction magnitude of TAPM relative to conventional asphalt pavement material, °C.

3.2 Cooling efficiency contributions to field performance

The asphalt materials are subjected to the cyclic impacts of temperature field when serving in the pavement. Since the viscoelastic response and aging rate of asphalt materials are tightly related to the factor of temperature, the excessively high service temperature of asphalt pavement in summer can give rise to the more serious high-temperature instability and aging degree for asphalt materials. In this case, the cooling effect of TAPM has the potential to improve the relevant field performance of asphalt pavement materials through lowering the service temperature of asphalt pavement in summer.

3.2.1 The action modes of cooling effect on field performance

According to the viscoelastic theory and aging regularity of asphalt materials, the temperature differences between the thermochromic asphalt pavement and conventional asphalt pavement within daily high-temperature period should be particularly concerned.

It is known that the temperature reduction magnitude of TAPM relative to conventional asphalt pavement material is not a constant value but continually varies with the meteorological data every moment. For simplicity, the action modes of cooling effect on field performance were determined based on the specimen temperature data

monitored in outdoor solar radiation test (shown as Fig. 5 (a)). Herein, the average results of three-day specimen temperature curves were taken as the representative service temperatures for modified and control samples in summer, and are presented in Fig. 10. It can be observed that the temperature differences between the modified and control samples mainly occur within the high-temperature period from 11:00 a.m. to 4:00 p.m. With the specimen temperatures no longer largely fluctuating, both the modified and control samples approximately reach the thermal equilibrium within the period from 1:30 p.m. to 3:00 p.m. During this period, the temperature inside the modified sample is about 56 °C while the temperature inside the control sample is about 61°C, with the temperature difference of 5 °C.

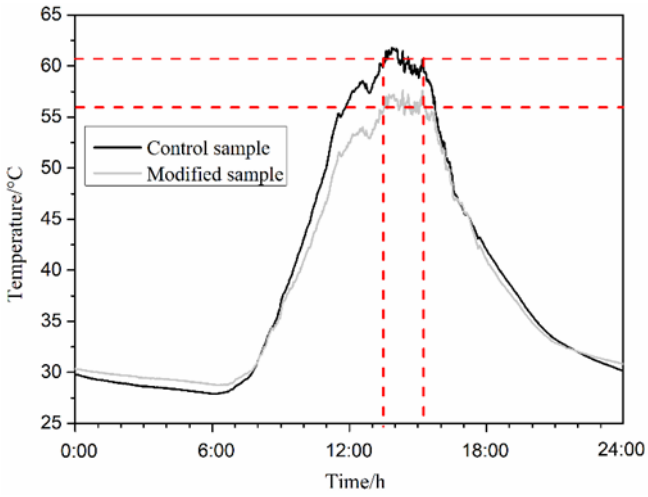

Fig. 10. The average results of three-day specimen temperature curves in outdoor solar radiation test [23]**.**

In view of the cooling characteristics of modified sample relative to control sample as well as the relationship between field performance of asphalt mixture and temperature, the action modes of cooling effect on different field performance are specified as follows.

In the case of high-temperature performance evaluation, two scenarios were analyzed. One is that without consideration of cooling effect, the dynamic modulus master curves of modified and control samples were compared with each other at the same temperature of 50 °C. Another is that with consideration of cooling effect, the dynamic modulus master curve of modified sample at 56 °C was compared with that of control sample at 61 °C. Additionally, the real-time dynamic moduli of modified and control samples corresponding to their respective field service temperature curves were also compared. As for the evaluation of aging and low-temperature performance, both modified and control samples were classified into two groups. One was the aged group in which the modified and control samples were aged in oven for 15 days at 61 °C and 56 °C, respectively. Another was the unaged group. Thereafter, the performance differences between modified and control samples were compared before and after aging.

It should be explained that the high-temperature instability of asphalt mixture is a premature distress, and thereby the samples were not treated with oven aging process before the high-temperature performance was evaluated. Instead, the aging is one of the primary contributors to the cracking distresses [41, 42], so that the oven aging processes under respective thermal equilibrium temperatures were conducted on modified and control samples before the evaluation of relevant performance. The aging of asphalt materials mainly occurs within daily high-temperature duration. Therefore, the aging time was set to be 15 days based on the assumption that the summer has three months and the high-temperature duration is lasted for 4 hours every day.

3.2.2 High-temperature stability

The comparison results of dynamic modulus master curves of modified and control samples in two scenarios are shown in Fig. 11. At the same temperature, the dynamic moduli of modified sample are lower than those of control sample especially at lower frequencies, indicating the control sample has a better high-temperature stability than the modified sample when the cooling effect of modified sample is ignored. Instead, the dynamic moduli of modified sample outweigh those of control sample in consideration of the cooling effect. This indicates a service temperature reduction of 5 °C brought by the cooling effect of modified sample can make up for its own deficiency in high-temperature stability, and make the high-temperature stability of modified sample better than that of control sample in real field service.

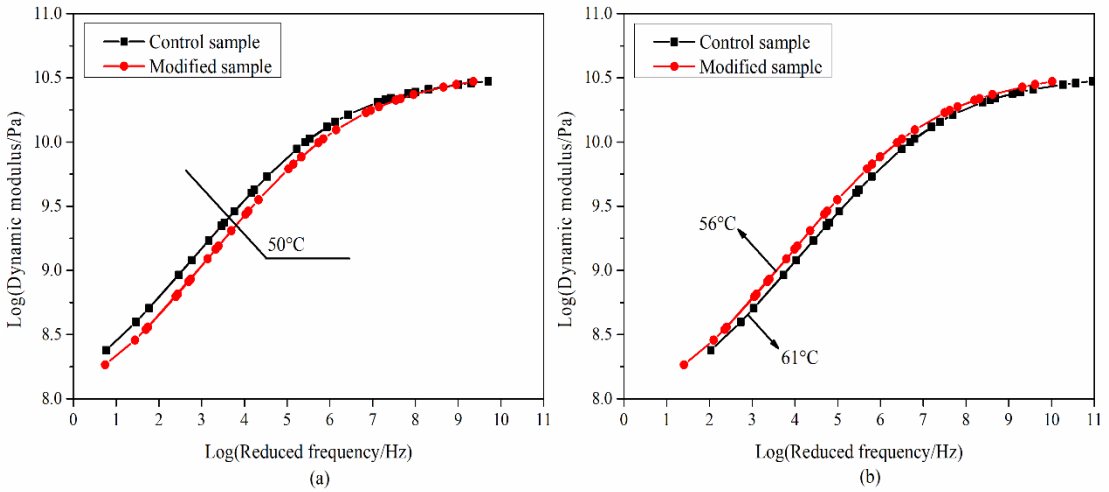

Fig. 11. The comparisons of dynamic modulus master curves of modified and control samples: (a) without consideration of cooling effect and (b) with consideration of cooling effect.

For further quantitative illustration, the dynamic modulus at 1.59 Hz was extracted and the dynamic modulus change rate (DMCR) of modified sample relative to control

sample is defined according to equation (26). As shown by Fig. 12, the DMCR is increased from -19.0% to 12.4%, with an increase of more than 30%, when the cooling effect is considered. The substantial improvement in this relative value further demonstrates the contribution of cooling effect of TAPM to the high-temperature stability of asphalt mixture.

$$\mathrm{DMCR} = \frac{\text{Dynamic modulus}_{\text{Modified sample}} - \text{Dynamic modulus}_{\text{Control sample}}}{\text{Dynamic modulus}_{\text{Control sample}}} \times 100\% \qquad (26)$$

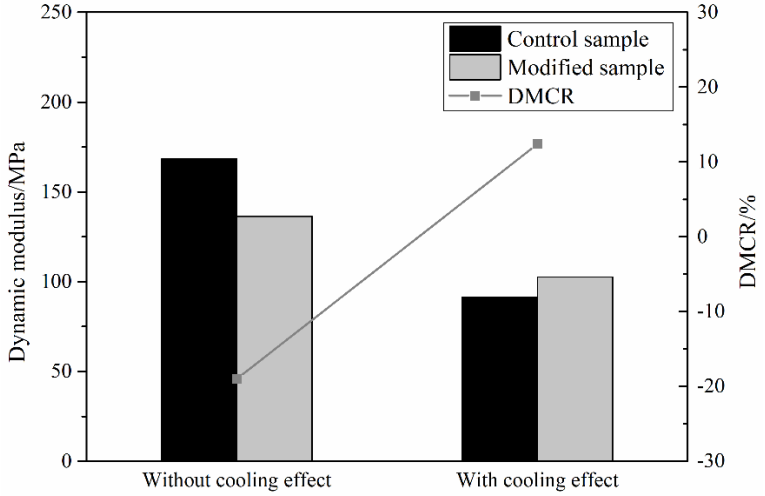

Fig. 12. Comparisons of dynamic modulus at 1.59 Hz of modified and control samples without and with consideration of cooling effect.

The real-time dynamic moduli of modified and control samples in accordance with their respective field service temperature curves (shown in Fig. 10) are presented in Fig. 13. The dynamic modulus presents a negative correlation with the service temperature, for both modified and control samples. From 11 a.m. to 3:30 p.m., the dynamic modulus largely decreases first and then slightly increases, and reaches the minimum value at the time of around 2:00 p.m. The DMCR values of modified sample relative to control sample at every service moment are also presented. The DMCR starts to gradually increase from 11 a.m., and reaches the maximum value of 35% at 2:00 p.m. Furthermore,

the DMCR values are always larger than 20% within the daily high-temperature period from 12:00 a.m. to 3:30 p.m. This further demonstrates during the real field service, the modified sample, due to its cooling effect, is able to possess a much better high-temperature stability than control sample. This result is contrary to the case in which the cooling effect is neglected. Therefore, it can be concluded that considering the cooling effect is beneficial to a more objective evaluation of high-temperature stability of TAPM.

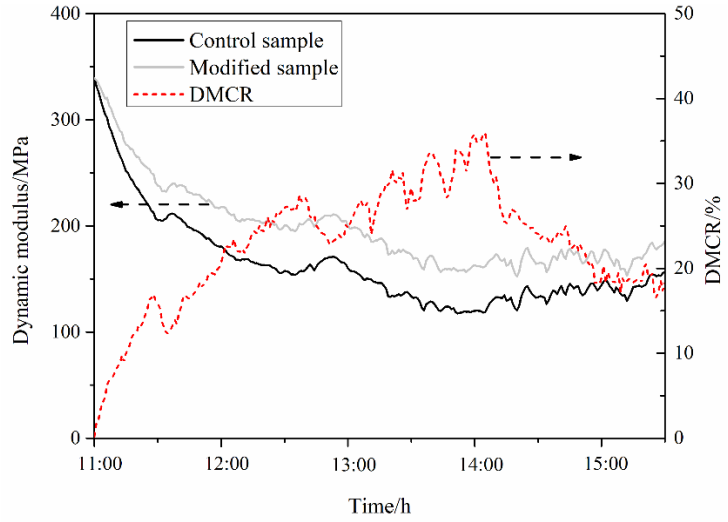

Fig. 13. Comparisons of real-time dynamic moduli of modified and control samples corresponding to their respective field service temperature curves [23]**.**

3.2.3 Aging resistance

The dynamic modulus master curves (at 20 °C) of modified and control samples before and after aging are illustrated in Fig. 14. For the modified sample, there is almost no obvious change in dynamic modulus master curves before and after aging. In comparison, the dynamic modulus master curve of control sample moves upwards significantly after aging. This means the aging phenomenon of control sample is much more serious than that of modified sample when modified and control samples are

simultaneously exposed to the same outdoor environment in summer. A service temperature reduction of 5 °C of modified sample relative to control sample can be responsible for the aging degree discrepancy between them. The aging rate of asphalt materials presents the positive correlation with temperature, especially within high temperature range [43], so that the cooling effect of modified sample within daily high-temperature period can effectively alleviate the age hardening degree of asphalt mixture.

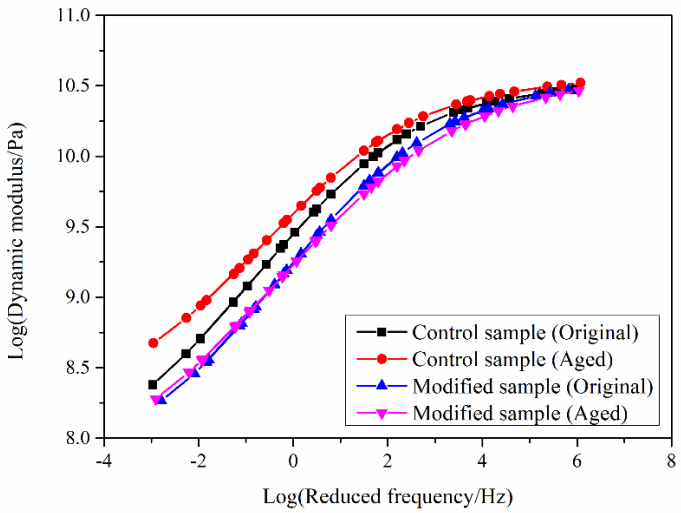

Fig. 14. Dynamic modulus master curves (at 20 °C) of modified and control samples before and after aging.

The relaxation spectrum can be regarded as the “fingerprint” of viscoelastic information of asphalt mixture [38]. Therefore, the variation of relaxation spectrum before and after aging can be also employed to evaluate the aging effect on asphalt mixture. As shown in Fig. 15, both continuous and discrete relaxation spectra of modified sample do not significantly change before and after aging, while the relaxation strength in continuous and discrete spectra largely increases after aging for control sample, especially within the shorter relaxation time range. This phenomenon further indicates there indeed exists the aging degree discrepancy between modified and

control samples after cyclic effects of thermal environment in summer, and the cooling effect of modified sample can mitigate the aging degree of asphalt mixture during this period.

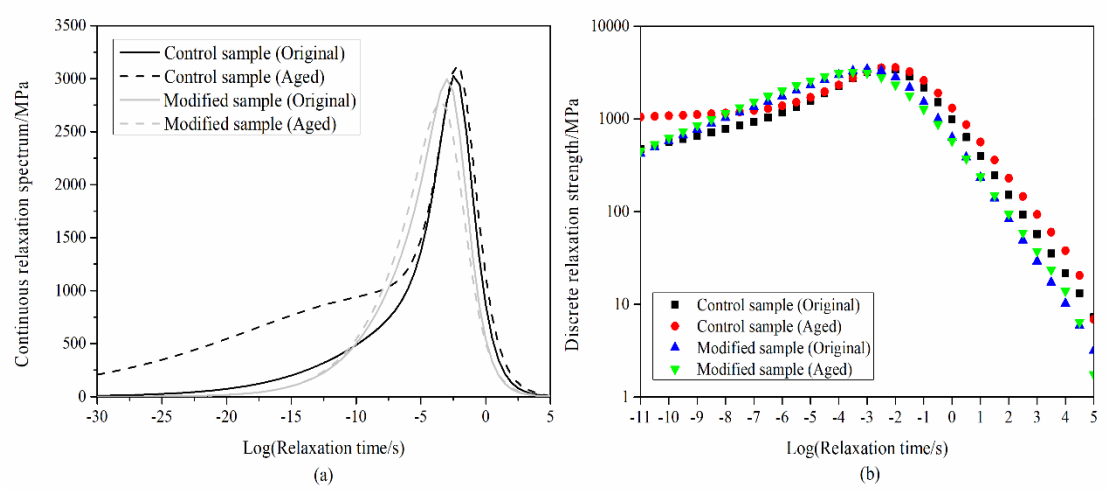

Fig. 15. Relaxation spectra (at 20 °C) of modified and control samples before and after aging: (a) continuous relaxation spectrum and (b) discrete relaxation spectrum.

3.2.4 Low-temperature cracking resistance

The relaxation modulus is commonly used to evaluate the stress relaxation ability of asphalt mixture. A smaller relaxation modulus indicates a better relaxation ability. Relaxation modulus master curves of modified and control samples before and after aging are illustrated in Fig. 16. Irrespective of sample types, the relaxation modulus decreases with the growth of relaxation time in general, indicating the intrinsic relaxation behavior of asphalt mixture. In original state, the discrepancies of relaxation modulus master curves between modified and control samples are not significant. After aging, the relaxation modulus master curve of control sample moves upwards largely while the relaxation modulus master curve of modified sample seldom changes, so that

the discrepancies between them become much evident. The cooling effect contribution to the improvement in asphalt mixture stress relaxation ability is mainly manifested after asphalt mixtures are aged by photo-thermal environment of summer for a certain period. This can be explained by the fact that the cooling effect of modified sample can alleviate the age hardening degree of asphalt mixture during the high-temperature period in summer.

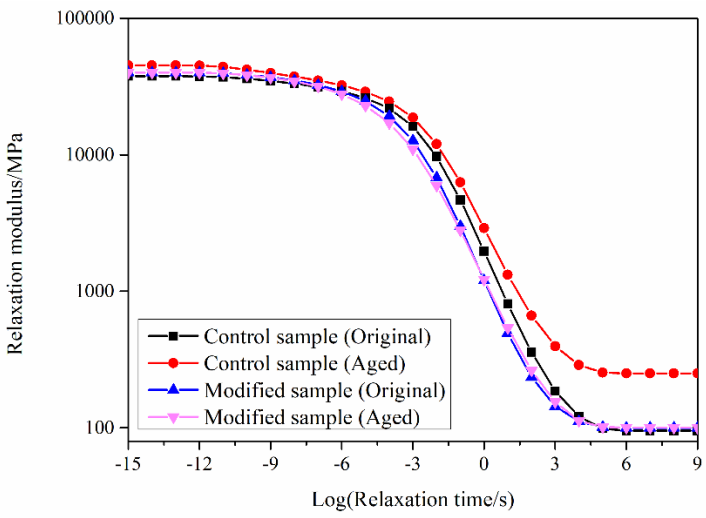

Fig. 16. Relaxation modulus master curves (at 20 °C) of modified and control samples before and after aging.

The thermal stress change rate (TSCR) of modified sample relative to control sample is defined according to equation (27). Additionally, the accumulated thermal stresses in samples as well as TSCR values during cooling process before and after aging are presented in Fig. 17. Although the thermal stresses in all samples are increased after aging, the increase magnitude for modified sample is much less than that for control sample. As a result, the TSCR values are further substantially reduced after aging, as shown by two dashed lines in Fig.17. The advantage of modified sample over control sample in thermal stress relaxation performance is significantly expanded after

aging.

$$\mathrm{TSCR} = \frac{\text{Thermal stress}_{\text{Modified sample}} - \text{Thermal stress}_{\text{Control sample}}}{\text{Thermal stress}_{\text{Control sample}}} \times 100\% \quad (27)$$

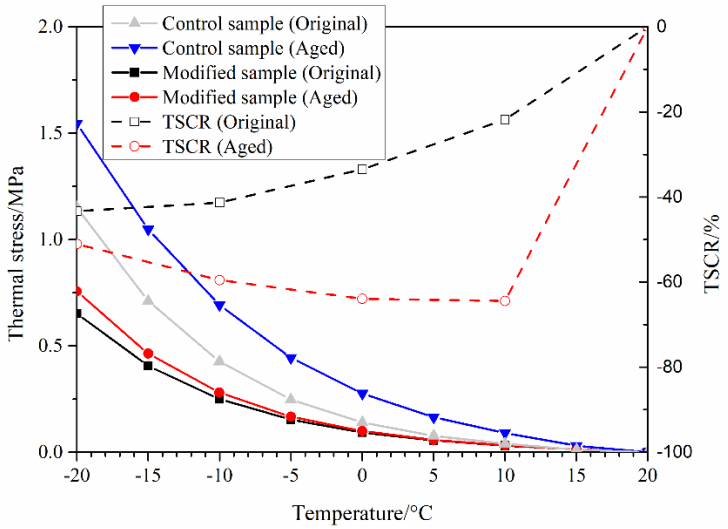

Fig. 17. The accumulated thermal stresses in samples as well as TSCR values during cooling process before and after aging.

Failure tensile strain (FTS) results of modified and control samples before and after aging are illustrated in Fig. 18. The failure tensile strain change rate (FTSCR) of modified sample relative to control sample is defined as per equation (28). The difference of FTS between modified and control samples is minor before aging. Due to the aging impact, the FTS of control sample is greatly reduced by 27.7% while the value of modified sample is only reduced by 5.5%, so that the FTSCR is correspondingly increased by 30%. It is the aging degree discrepancy between modified and control samples during the high-temperature period in summer that leads to their disparity in low-temperature deformation ability.

$$\mathrm{FTSCR} = \frac{\mathrm{FTS}_{\text{Modified sample}} - \mathrm{FTS}_{\text{Control sample}}}{\mathrm{FTS}_{\text{Control sample}}} \times 100\% \quad (28)$$

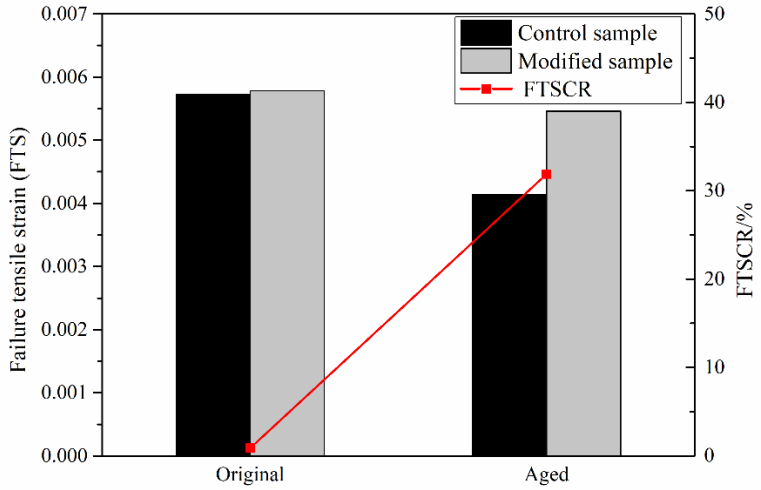

Fig. 18. Failure tensile strain results of modified and control samples before and after aging.

4. Conclusions

In this study, the cooling efficiency of thermochromic asphalt material to pavement in hot summertime was verified through the experimental test combined with numerical simulation. Additionally, the effects of the cooling function of thermochromic asphalt material on the field performance of asphalt mixture were investigated. The major findings of this research are summarized as follows:

- Through the interpolation and back-calculation methodologies, the solar albedo of thermochromic asphalt pavement material is determined to be 0.30 that is six times larger than that of conventional asphalt pavement material. The solar radiation reflection ability of asphalt pavement material is effectively enhanced due to the modification effect of thermochromic microcapsule.
- Based on the calculated thermophysical parameters as well as the real meteorological conditions, the average cooling magnitude of thermochromic asphalt pavement relative to conventional asphalt pavement in ten different regions

are numerically calculated to be 6.26 ℃, with a standard deviation of 0.79 ℃. The thermochromic asphalt pavement material is able to take the effective, universal and stable cooling effect on pavement in summer across China.

- Although the dynamic modulus of thermochromic asphalt mixture is smaller than that of conventional asphalt mixture at the same testing temperature, the results of real-time dynamic moduli curves indicate the thermochromic asphalt mixture, due to its cooling effect, is able to possess a much better high-temperature stability than conventional asphalt mixture during the real field service in summer.
- The aging degree of asphalt mixture deepens after cyclic effects of thermal environment in summer, but the cooling effect of thermochromic asphalt pavement material within daily high-temperature period can effectively alleviate the age hardening degree of asphalt mixture.
- The cooling effect of thermochromic asphalt pavement material can indirectly improve the thermal stress relaxation ability and low-temperature deformation capacity of asphalt mixture through reducing the aging degree of asphalt mixture during the high-temperature period of summer.

5. Recommendations for future work

In this research, the relationship between the cooling function of TAPM and its field performance was discussed. In future research, the influence of cooling function of this paving material on the temperature and modulus distribution inside pavement structure as well as the pavement mechanical response and service life will be systematically investigated, and the pavement design theory for the pavement built with

TAPM will be developed.

Acknowledgments

This work was supported by National Natural Science Foundation of China (grant number 52078209), Hunan Provincial Natural Science Foundation of China (grant number 2022JJ30155), Transportation Science and Technology Development and Innovation Project of Hunan Province (grant number 201805) and Science and Technology Planning Project of Hunan Province (grant number 2018TP2038). The authors gratefully acknowledge their financial support.

References

[1] Pan P, Wu SP, Xiao Y, Liu G. A review on hydronic asphalt pavement for energy harvesting and snow melting. Renew Sustain Energy Rev 2015;48:624–634.

[2] Aletba SRO, Hassan NA, Jaya RP, Aminudin E, Mahmud MZH, Mohamed A, Hussein AA. Thermal performance of cooling strategies for asphalt pavement: a state-of-the-art review. J Traffic Transport Eng 2021;8(3):356–373.

[3] Wang B, Hu XD, Cao CF, Wan JM, Gan WX, Chen ZW, Cai CL. Development and characterization of permeative anti-rutting agent for asphalt mixture enhancement. Construct Build Mater 2023;364:129937.

[4] Zeng WB, Wu SP, Wen J, Chen ZW. The temperature effects in aging index of asphalt during UV aging process. Construct Build Mater 2015;93:1125–1131.

[5] Hung AM, Kazembeyki M, Hoover CG, Fini EH. Evolution of morphological and nanomechanical properties of bitumen thin films as a result of compositional changes due to ultraviolet radiation. ACS Sustain Chem Eng 2019;7:18005–18014.

[6] Mohajerani A, Bakaric J, Jeffrey-Bailey T. The urban heat island effect, its causes, and mitigation, with reference to the thermal properties of asphalt concrete. J Environ Manag 2017;197:522–538.

[7] Qin YH. A review on the development of cool pavements to mitigate urban heat island effect. Renew Sustain Energy Rev 2015;52:445–459.

[8] Santamouris M. Using cool pavements as a mitigation strategy to fight urban heat island-A review of the actual developments. Renew Sustain Energy Rev 2013;26: 224–240.

[9] Santamouris M, Gaitani N, Spanou A, Saliari M, Giannopoulou K, Vasilakopoulou K, Kardomateas T. Using cool paving materials to improve microclimate of urban areas-design realization and results of the flisvos project. Build Environ 2012;53 (7):128–136.

[10] Xu L, Wang JY, Xiao FP, Ei-Badawy S, Awed A. Potential strategies to mitigate the heat island impacts of highway pavement on megacities with considerations of energy uses. Appl Energy 2021;281:116077.

[11] Liu PF, Kong XR, Du C, Wang CH, Wang D, Oeser M. Numerical investigation of the temperature field effect on the mechanical responses of conventional and cool pavements. Materials 2022;15(19):6813.

[12] Sun YR, Du C, Gong HR, Li YH, Chen JY. Effect of temperature field on damage initiation in asphalt pavement: A microstructure based multiscale finite element method. Mech Mater 2020;144:103367.

[13] Gui J, Phelan PE, Kaloush KE, Golden JS. Impact of pavement thermophysical

properties on surface temperatures. J Mater Civ Eng 2007;19:683–690.

[14] Rossi F, Pisello AL, Nicolini A, Filipponi M, Palombo M. Analysis of retro-reflective surfaces for urban heat island mitigation: A new analytical model. Appl Energ 2014;114:621–631.

[15] Synnefa A, Karlessi T, Gaitani N, Santamouris M, Assimakopoulos DN, Papakatsikas C. Experimental testing of cool colored thin layer asphalt and estimation of its potential to improve the urban microclimate. Build Environ 2011; 46:38–44.

[16] Testa J, Krarti M. A review of benefits and limitations of static and switchable cool roof systems. Renew Sust Energ Rev 2017;77:451–460.

[17] Hu JY, Yu X. Experimental study of sustainable asphalt binder: influence of thermochromic materials. Transport Res Rec 2013;2372:108–115.

[18] Hu JY, Yu X. Innovative thermochromic asphalt coating: characterisation and thermal performance. Road Mater Pavement 2015;17(1):1–16.

[19] Tang H, Maclaren DC, White MA. New insights concerning the mechanism of reversible thermochromic mixtures. Can J Chem 2010;88(11):1063–1070.

[20] Karlessi T, Santamouris M, Apostolakis K, Synnefa A, Livada I. Development and testing of thermochromic coatings for buildings and urban structures. Sol Energy 2009;83(4):538–551.

[21] Hu JY, Gao Q, Yu X. Characterization of the optical and mechanical properties of innovative multifunctional thermochromic asphalt binders. J Mater Civ Eng 2015;27(5):04014171-1–04014171-10.

[22] Zhang J, Chen AS, Wang LH, Li XA, Huang W. Striving toward visible light photocatalytic water splitting based on natural silicate clay mineral: the interface modification of attapulgite at the atomic-molecular level. ACS Sustain Chem Eng 2016;4:4601–4607.

[23] Chen ZH, Liu JX, Zhang HL, Kuang HP, Zhao MT, Zhang S. Comparative investigation of mechanical and cooling performance between thermochromic road materials prepared by wet/dry process: For low-carbon production and sustainable service. J Clean Prod 2022;360:132158.

[24] Li Q, Jiang JW, Hu TY, Meng YP, Gao L, Luo S. Laboratory evaluation of rutting resistance for asphalt binders and mixtures modified with different thermochromic microcapsule powders. Construct Build Mater 2020;252:119099.

[25] Li Q, Hu TY, Luo S, Gao L, Wang CH, Guan YS. Evaluation of cooling effect and pavement performance for thermochromic material modified asphalt mixtures under solar radiation. Construct Build Mater 2020;261:120589.

[26] Yu B, Peng WZ, Liu JZ, Zhang JY, Li W, Hong QZ. Research on the performance of temperature responsive asphalt mixture with thermochromic material. Road Mater Pavement 2022;23(3):713–724.

[27] Chen ZH, Zhang HL, Duan HH, Shi CJ. Improvement of thermal and optical responses of short-term aged thermochromic asphalt binder by warm-mix asphalt technology. J Clean Prod 2021;279:123675.

[28] Hu JY, Yu X. Performance evaluation of solar-responsive asphalt mixture with thermochromic materials and nano-TiO_2 scatterers. Construct Build Mater 2020;

247:118605.

[29] Richard C, Dore G, Lemieux C, Bilodeau JP, Haure-Touze J. Albedo of pavement surfacing materials: in situ measurements. In Proceedings: Cold Regions Engineering 2015;181–192.

[30] García Mainieri JJ, Sen S, Roesler J, Al-Qadi IL. Albedo change mechanism of asphalt concrete surfaces. Transport Res Rec 2022;2676(7):763–772.

[31] Yang X, Zhang HL, Zheng WZ, Chen ZH, Shi, CJ. A novel rejuvenating method for structural and performance recovery of aged SBS-modified bitumen. ACS Sustain Chem Eng 2022;10(4):1565–1577.

[32] Li DN, Leng Z, Zhang SW, Jiang JW, Yu HY, Wellner F, Leischner S. Blending efficiency of reclaimed asphalt rubber pavement mixture and its correlation with cracking resistance. Resour Conserv Recy 2022;185:106506.

[33] Wang HP, Liu XY, Zhang H, Apostolidis P, Erkens S, Skarpas A. Micromechanical modelling of complex shear modulus of crumb rubber modified bitumen. Mater Design 2020;188:108467.

[34] Xu X, Leng Z, Lan JT, Wang W, Yu JM, Bai YW, Sreeram A, Hu J. Sustainable practice in pavement engineering through value-added collective recycling of waste plastic and waste tyre rubber. Engineering 2021;7:857–867.

[35] Du C, Sun YR, Chen JY, Zhou CJ, Liu PF, Wang DW, Oeser M. Coupled thermomechanical damage behavior analysis of asphalt pavements using a 2D mesostructure-based finite-element method. J Transp Eng Part B: Pavements 2021;147(2):04021012-1–04021012-13.

[36] Liu PF, Hu J, Wang H, Falla GC, Wang DW, Oeser M. Influence of temperature on the mechanical response of asphalt mixtures using microstructural analysis and finite-element simulations. J Mater Civ Eng 2018;30(12):04018327-1–04018327-14.

[37] Liao GY, Huang XM. 2014. Application of ABAQUS finite element software in road engineering; Southeast University Press: Nanjing, China.

[38] Zhang Y, Sun YR. Fast-acquiring high-quality prony series parameters of asphalt concrete through viscoelastic continuous spectral models. Materials 2022;15(3): 716.

[39] Xu JQ, Yang EH, Luo HY, Ding HB. Effects of warm mix additives on the thermal stress and ductile resistance of asphalt binders. Construct Build Mater 2020;238: 117746.

[40] Hu JY, Yu X, Tao JL. Innovative chromogenic materials for pavement life extension: modeling study of surface temperature of sustainable asphalt pavement. Int J Pavement Res Technol 2013;6(2):141-145.

[41] Behnood A. Application of rejuvenators to improve the rheological and mechanical properties of asphalt binders and mixtures: A review. J Clean Prod 2019;231:171–182.

[42] Zhang HL, Chen ZH, Xu GQ, Shi CJ. Evaluation of aging behaviors of asphalt binders through different rheological indices. Fuel 2018;221:78–88.

[43] Liu F, Zhou ZD, Zhang X, Wang Y. On the linking of the rheological properties of asphalt binders exposed to oven aging and PAV aging. Int J Pavement Eng

2021;22(3):331–340.